High Voltage High Brightness Electron Accelerator with MITL Voltage Adder Coupled to Foilless Diode

Michael G. Mazarakis, J. W. Poukey, D. Rovang, S. Cordova, P. Pankuch,
R. Wavrik, D. L. Smith, J. E. Maenchen, L. Bennett, K. Shimp, and K. Law
Sandia National Laboratories
P. O. Box 5800
Albuquerque, NM 87185-1193

Abstract

The design and analysis of a high brightness electron beam experiment under construction at Sandia National Laboratory is presented. The beam energy is 12 MeV, the current 35-40 kA, the rms radius 0.5 mm, and the pulse duration FWHM 40 ns. The accelerator is SABRE [J. Corley, J. A. Alexander, P. J. Pankuch, C. E. Heath, D. L. Johnson, J. J. Ramirez, and G. J. Denison, in *Proceedings of the Eighth International IEEE Pulsed Power Conference*, San Diego, CA, 1991 (IEEE, New York, 1991), p. 920], a pulsed inductive voltage adder, and the electron source is a magnetically immersed foilless diode. This experiment has as its goal to stretch the technology to the edge and produce the highest possible electron current in a submillimeter radius beam.

Introduction

During the last 15 years, Sandia National Laboratories dedicated a considerable effort toward developing ultra high current and high brightness electron beams. The energy range was between 4 MeV and 20 MeV and the current was 30-100 kA. The accelerators utilized were single pulse devices, which can be divided into two groups: the single stage Blumlein-type accelerators such as Hermes II[1] and IBEX,[2] and the multistage devices such as RADLAC I,[3] RADLAC II,[4] RADLAC II/SMILE[5], and MABE.[6]

The electron source of choice was the magnetically immersed foilless diode.[7] This diode is ideally suited to produce high current and high brightness beams. The beams are generated and propagated in a strong axial magnetic field; thus, large amounts of current can be contained and tightly focused in small radius cross sections with relatively very small transverse velocities.

The present experiments were motivated by the success of converting RADLAC II into an inductive voltage adder fitted with a magnetically immersed foilless diode (RADLAC II/SMILE). The RADLAC II accelerator in its original configuration was an electron induction linear accelerator designed to produce ~ 100 kA, 16 MeV electron beams. The beam was produced by a magnetically immersed foilless diode located at the lower voltage end of the device (4-MV injector). It was then transported magnetically and further accelerated through the remaining six postaccelerating gaps of 2-MV accelerating voltage each. The SMILE modification converted RADLAC II into an inductive voltage adder similar to Hermes III[8] and SABRE.[9] The RADLAC II/SMILE configuration had a higher, 150 ohm, impedance which matched the original linac impedance. It proved that an inductive voltage adder can successfully be coupled to a magnetically immersed foilless diode

DISCLAIMER

Portions of this document may be illegible
in electronic image products. Images are
produced from the best available original
document.

to produce high quality electron beams. Annular beams of 50-100 kA, 1 cm radius were produced with very sharply defined 3-mm thick annulus and low transverse velocities ($\beta_\perp \approx 0.05$).

The beam experiments described here utilize the SABRE accelerator modified to a higher impedance voltage adder ($\sim$ 120 ohm) and fitted with a foilless diode immersed in a very strong (23 Tesla) solenoidal magnetic field.

In the next sections, the SABRE accelerator and the design which modifies it to a higher impedance voltage adder, the magnetically immersed foilless diode, and numerical simulation analysis of the produced e⁻ beam properties are presented.

SABRE Modifications

The SABRE accelerator (Fig. 1) design is based on the successful Hermes-III technology developed at Sandia during the last ten years in collaboration with Pulse Sciences Inc. this technology is fairly simple and couples the self-magnetically insulated transmission line (MITL)[10] principle with that of the induction linac[11] to generate a new family of linear induction accelerators, which we call linear inductive voltage adders. In these accelerators, the particle beam which drifts through the multiple cavities of conventional induction linacs is replaced by a metal conductor which extends along the entire length of the device and effectuates the voltage addition of the accelerating cavities. These devices can operate in either polarity to produce negative or positive voltage pulses. In a negative polarity voltage adder (Fig. 2), the center conductor is negatively charged relative to the outer conductor which is interrupted at regular intervals by the cavity gaps. SABRE in its original configuration is a relatively low impedance inductive voltage adder (Fig. 3). It was designed to operate in negative polarity at 40 ohm maximum output impedance and in positive polarity at approximately 20 ohm. It has 10 inductively insulated cavities each rated to maximum voltage of 1.2-1.3 MV. Ideally SABRE should be able to produce a 12-MV, 300-kA output in negative polarity and $\sim$ 8 MV, 400 kA in positive polarity. Because of higher than expected energy losses in the pulse forming network, the operating input cavity voltage is of the order of 800 kV which limits the total output voltage to $\sim$ 8 MV for negative polarity and 6 MV for positive polarity.

The modifications proposed here aim to increase the output voltage in both polarities and reduce the current proportionally since we do not plan to increase the total energy stored in the device. SABRE's main energy storage section consists of a Marx generator, two intermediate store capacitors and two energy transfer switches. Each switch controls the charging of ten pulse forming lines. Each cavity is fed by two 7.8-ohm pulse forming and transmission lines. The only major modification of the pulse forming network is the reduction of the total number of pulse forming and transmission lines into half (from 20 to 10). Thus, each cavity is fed by only one pulse forming line.

In addition, because each intermediate store will now feed power to only five pulse forming lines, the intermediate store-pulse forming line ringing ratio will substantially increase providing to the transmission lines and to the cavities a voltage pulse of $\sim$ 50% higher amplitude ($\sim$ 1.2 MV). With this modification we

have increased the impedance and the output voltage of each cavity. To take advantage of and maintain the voltage increase all the way to the output of the voltage adder, we must also increase the voltage adder impedance. To that effect a new smaller diameter cathode electrode was designed and constructed. Normally the impedance of the voltage adder is matched to that of the cavities; however, here to maintain an additional capability of further increasing the voltage output, the impedance of the voltage adder is 40% higher. To avoid exceeding 1.2 MV per cavity the Marx generator must be charged to lower voltage (85 kV instead of the 95 kV presently used) and the transfer switches must be triggered to close at a lower voltage level, 2-2.2 mV, instead of the usual 2.6 to 2.8 MV.
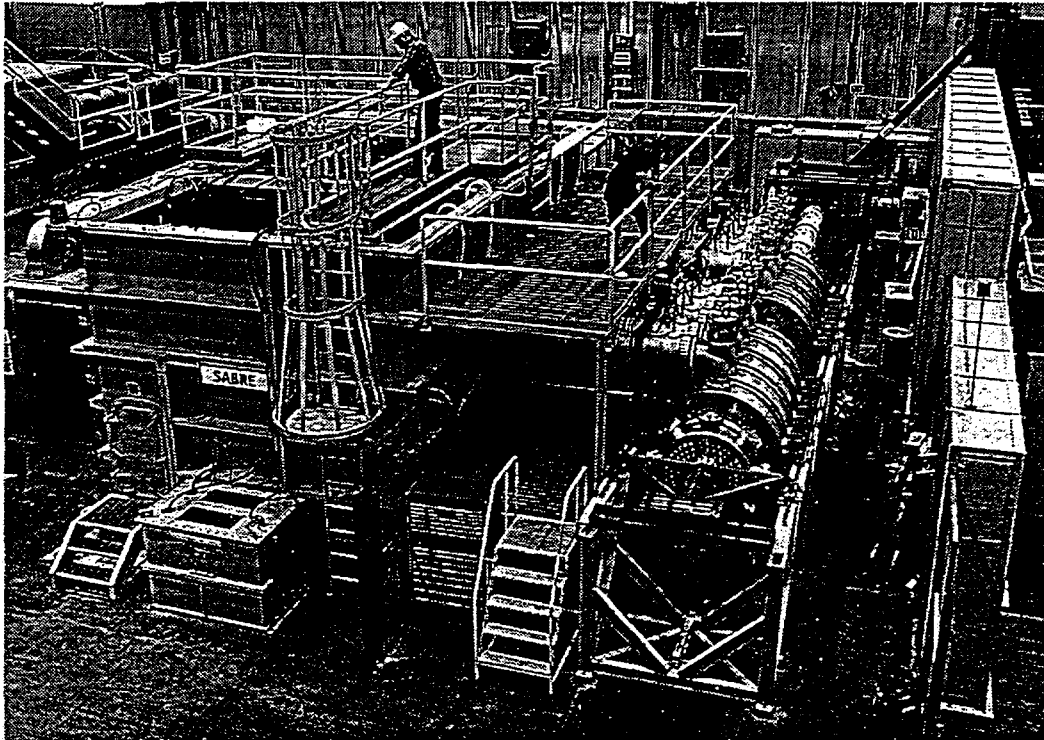

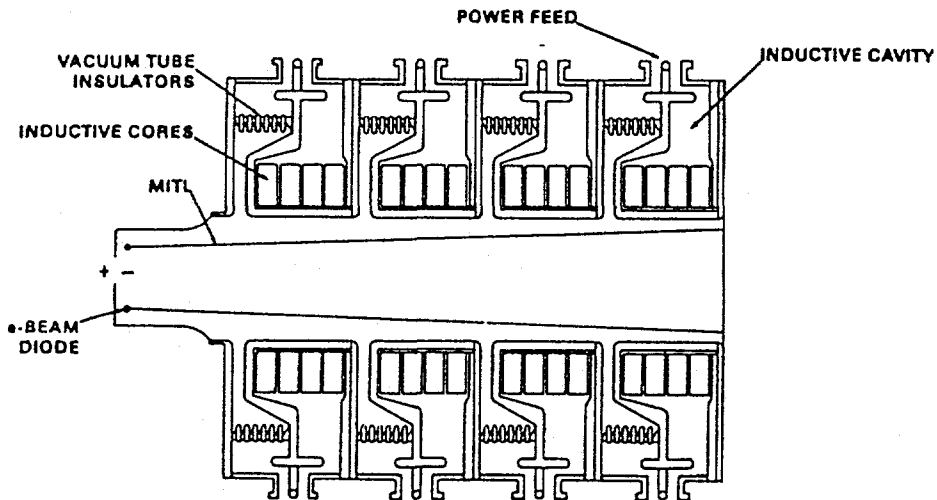Figure 1.   Photograph of SABRE accelerator

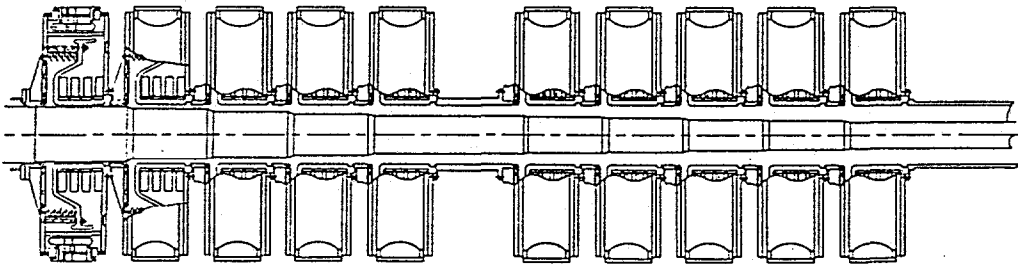Figure 2. A simple negative polarity voltage adder of the SABRE type

Figure 3. SABRE original low impedance voltage adder

The High Impedance MITL Design

The design of the high impedance voltage adder was done utilizing Creedon formalism.[10] It is based on a pulse forming line-fed self-magnetically insulated transmission line system which performs the series addition of voltage pulses from 10 cavity gaps (feeds). The cathode geometry is shown in Fig. 4. It is preferred over a continuous taper for the following reasons: it is easier and cheaper to manufacture, the constant radius segments provide constant vacuum impedance along each MITL segment, and the impedance increases gradually at each successive voltage feed with a rate of increase which follows the voltage axial gradient along the feed. The latter assures constant current flow over the entire length of SABRE.
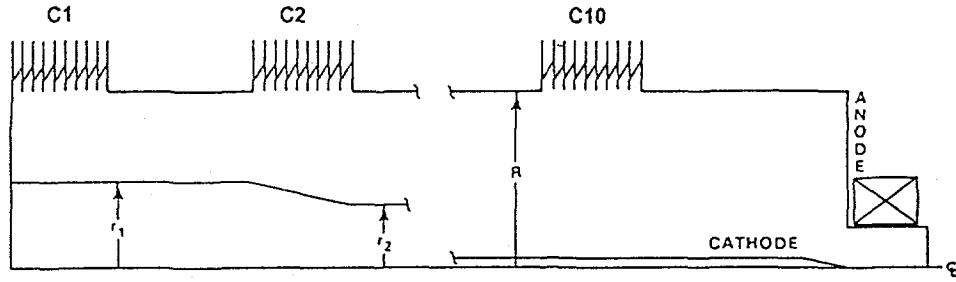
Figure 4. Schematic cross section of a high impedance voltage adder illustrating key design parameters

The vacuum impedance Z_i of each section i depends only on the dimensions of Fig. 4 and can be easily calculated from the following expression:

$$Z_i = 60 \ \ln(R / r_i)[\Omega]; \ i = 1,2, \ ....8 \tag{1}$$

where R = 19 cm and is the anode inner radius and r_i is the radius of the i-th cathode segment. The selection of the radius r_i of each cylindrical section was done in a fashion to provide the same operating load impedance for all of the SABRE cavity feeds. Some small variations were allowed for mechanical and construction reasons (see Table I for actual cathode radius).

The point design is for 110 kA and assumes equal 1.2 MV voltages at each cavity feed. Because of the relatively short voltage pulse (40-ns FWHM) of each feed, the current flow is self limited and, to a considerable extent, independent of the diode impedance conditions. However, in our design we stayed as close as possible to the constant current conditions all the way to the end of the cathode electrode. Near the upstream edge of the solenoid (Fig. 5) the cathode electrode smoothly tapers to accept the 1-mm cathode electrode of the immersed diode. Here the self-magnetic insulation is adiabatically replaced by the externally applied solenoidal field insulation. The anode inner radius is constant (19 cm) and defined by the existing SABRE anode cylinder. At first we determined the desired degree of overmatch of the MITL to the cavity feeds (~ 1.44). This in turn defined the operating impedance of each segment and the constant current I_ℓ of the voltage adder. With these initial parameters and Creedon equations for minimum current flow, I_ℓ, to establish self-limited magnetic insulation:

$$I_\ell = 8500 \ g\gamma_\ell^3 \ell n\left[\gamma_\ell + \left(\gamma_\ell^2 - 1\right)^{1/2}\right] ,$$

$$\gamma_i = \gamma_\ell + \left(\gamma_\ell^2 - 1\right)^{3/2} \ell n\left[\gamma_\ell + \left(\gamma_\ell^2 - 1\right)^{1/2}\right] , \tag{2}$$

$$g = \left[\ln R / r_i\right]^{-1} \text{ and } \gamma_i = V_i[MV] / mc^2 + 1 ,$$

we estimate the cathode radii and operating impedances of the entire new voltage adder for SABRE.
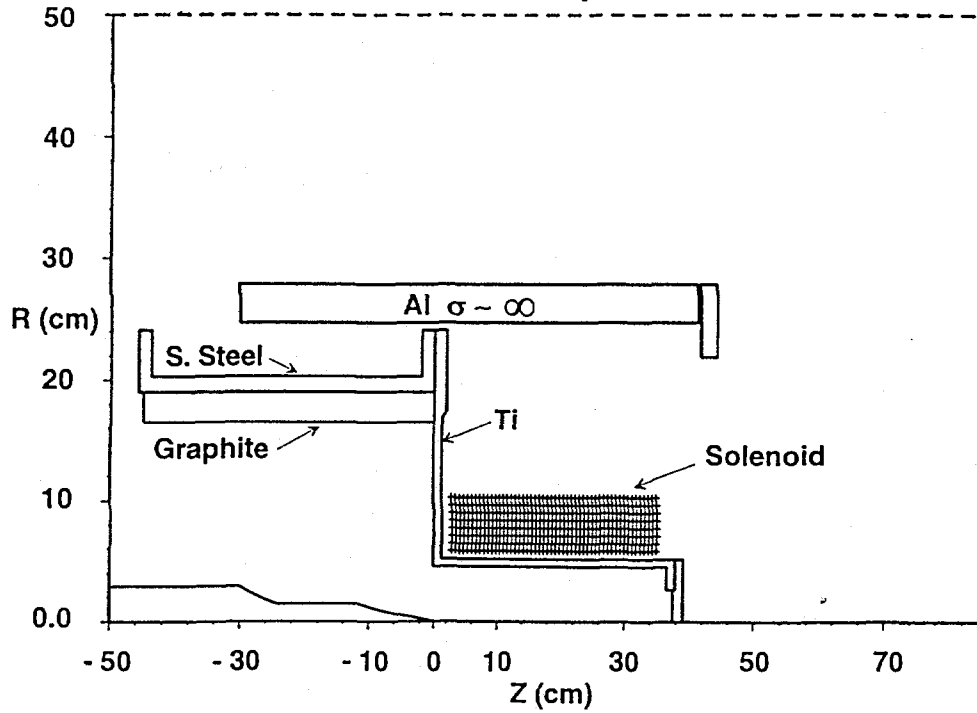
Figure 5. Schematic diagram of diode design and transition region

Our main concern was to keep the currents I_ℓ the same. The relativistic factor γ_ℓ is for electrons at the outer boundary of the electron sheath in the minimum current case. It can be approximated by the following formula which is tested to be correct[12] for up to 20 MV adders:

$$\gamma_\ell = \frac{12\ \gamma_i^{1/3}}{12 + \ell n \left[\dfrac{\gamma_i}{5.9314}\right]} \qquad (3)$$

Table I summarizes dimensions and design parameters. The cathode electrode (~ 9.2 m) includes the voltage adder section (6 m long) and a constant radius (2.2 cm) extension section (3.2 m long) and is cantilevered from the low voltage end of the accelerator. It starts with a 14-cm radius cylinder at the cathode end plate and tapers off to 2.2-cm radius after the 10th cavity gap (Fig. 6). Nine conical tapers were utilized along with 10 cylindrical sections and 11 flex-adjusting, double washer sections. The outer shell (anode cylinder) is formed by ten insulating stacks (feeds) alternating with ten cylinders, plus the final anode extension cylinder. The cathode electrode (Fig. 7) was preloaded before insertion into the anode cylinder to compensate for gravitational droop. The final adjustment was made in situ. Because of the large difference in radius between anode and cathode shank, precise alignment and centering of the cathode stock inside the anode cylinder is not very critical since the electrical potential is a logarithmic function of the radii.

Table I

Distance from cathode plate Z (cm)	Segment i (0 - 12)	Segment Voltage V_i (MV)	Cathode Radius R_c (cm)	Vacuum Impedance Z_i (Ω)	Operating Impedance Z_i (Ω)
0 - 33	0	0	13.65	20	11.6
37 - 80	1	1.2	13.65	20	11.6
84 - 127	2	2.4	10.95	33.2	22.6
131 - 174	3	3.6	8.41	49.0	35.3
178 - 221	4	4.8	7.14	58.9	44.4
225 - 366	5	6.0	5.715	72.2	55.5
370 - 413	6	7.2	4.76	83.2	65.0
417 - 460	7	8.4	3.81	96.6	76.6
464 - 507	8	9.6	3.175	107.5	86.3
511 - 554	9	10.8	2.54	120.9	98.1
558 - 900	10	12.0	2.22	129.0	105.5

R_{anode} = 19.05 cm
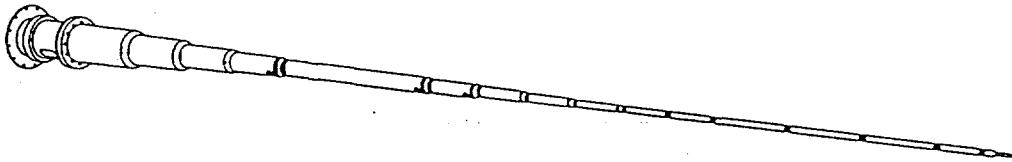
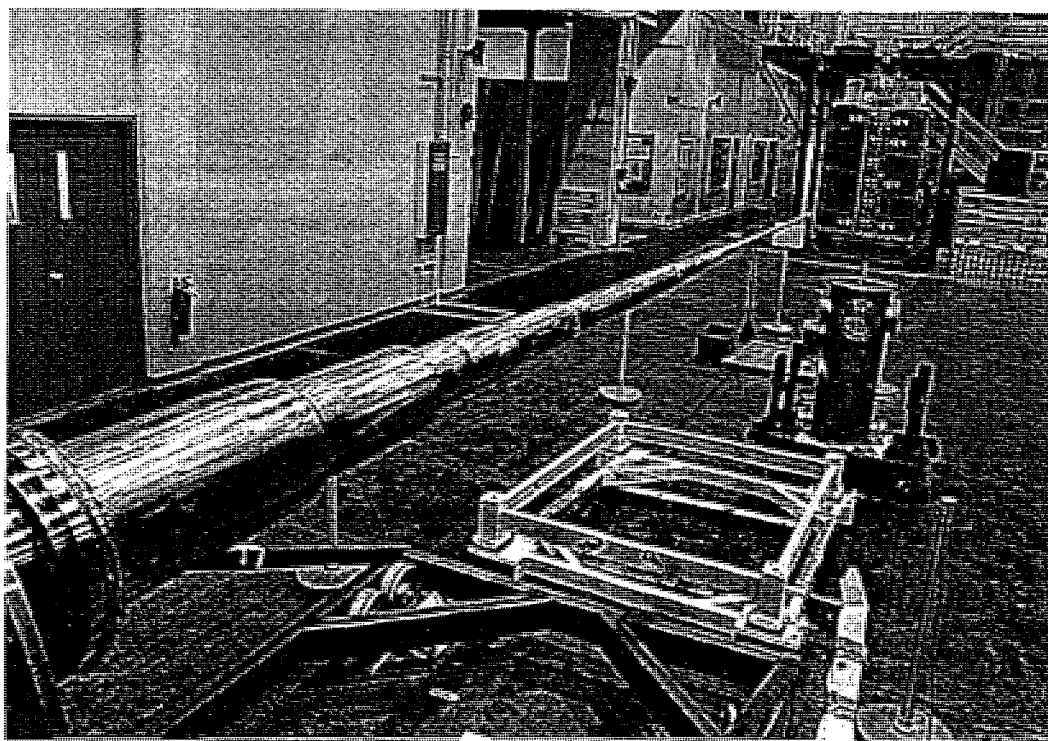Figure 6.   Line drawing of the new high impedance cathode electrode

Figure 7. Photograph of the cathode electrode. It is composed of 12 segments preloaded to compensate for the gravitation droop which is of the order of 20 cm.

Diode Design

The magnetically immersed foilless diode is similar to those of RADLAC II/SMILE and IBEX.[13] However, the impedance and solenoidal magnetic field are much higher. To generate beams of millimeter sizes the diode must be immersed in solenoidal fields of ~ 20 Tesla. A schematic diagram of the diode design including the solenoidal magnet is shown in Fig. 5. The anode and cathode electrodes are made of titanium because it is not magnetic material and has large resistivity, allowing the pulsed magnetic field to penetrate without appreciable losses.

The pulsed solenoids were designed and constructed in-house by our magnet team. They draw upon the large experience we acquired over many years of research and development for the high field coils of the inertial confinement fusion ion diodes. We have constructed four of them for redundance since we do not know yet their life time. These solenoids are among the strongest ever built. The total magnetic energy stored is ~ 1.8 MJ. The inductance is 8 mH, the bore 12 cm, and length is 30 cm. The shape of the fringe field is tailored by a 2-cm thick aluminum cylinder of 25-cm inner radius coaxially enclosing the entire diode assembly. The diode assembly and solenoids have been tested successfully to 23 Tesla. The magnetic field profile and strength (Fig. 8) are in good agreement with numerical simulation predictions done with our magnet code "Atheta." [14] The agreement is within the estimated measurement errors of 10%.
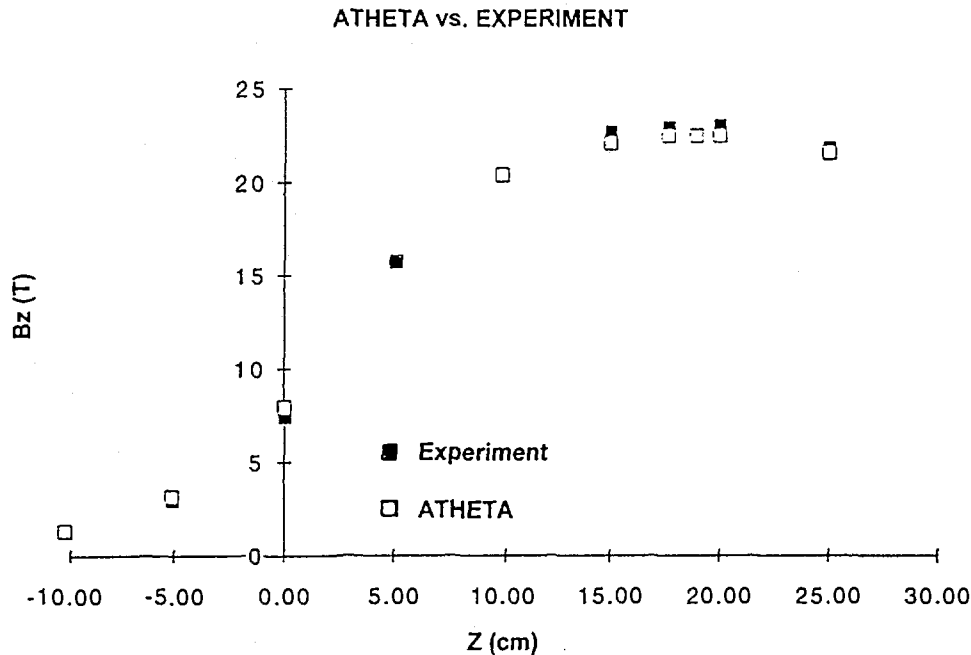
ATHETA vs. EXPERIMENT

Figure 8.   Measured and calculated magnetic field profile of the diode solenoid.

Simulation Results

The design of the MITL voltage adder (Table I) and the foilless diode (Fig. 5) were validated with a large number of TWOQUICK[15] particle-in-cell code simulations. Because of the large range in space and time scales, it was necessary to divide the entire design into three parts: voltage adder, from cavity feeds through the extension MITL to a (more or less) self-limited diode load; transition region where the coupling from MITL to immersed diode was studied; and finally, immersed diode where the beam generation and beam parameters were analyzed in fine detail. The optimum results are shown in Figures 9, 10, and 11. They go from the large scale of the entire SABRE voltage adder to the small scale of the immersed foilless diode and merge smoothly into one another.

Figure 9 shows an electron map at 60 ns following the arrival of the voltage pulse at the first cavity (t = 0). The line is magnetically insulated with the self-field (B_θ) of the current flowing along the voltage adder. Electron maps at earlier times (t = 20-30 ns) show some electron losses to the anode electrode. This is to be expected since self-limited magnetic insulated flow is established by driving some electron current to the anode wall during the rise time of the voltage pulse as it travels along the voltage adder. The anode-cathode gap of the planar diode at the end of the MITL is large, 20 cm, to allow operation in the self-limited mode. No applied magnetic field is assumed here. In this simulation, the cavity input voltage is a trapezoidal pulse of 1.2-MV peak value and 40-ns flat top (Fig. 9). Because the voltage adder is overmatched to the cavity impedance (12 ohm versus 7.8 ohm), the actual operating voltage pulse at the cavity gaps is higher, ~ 1.4 MV. These

pulses combine and travel down the voltage adder toward the slightly undermatched diode. The final voltage is 13 MV and the total current is 135 kA. The estimated operating impedance of 96 ohms agrees with the parapotential theory and pressure balance theory within 10%.
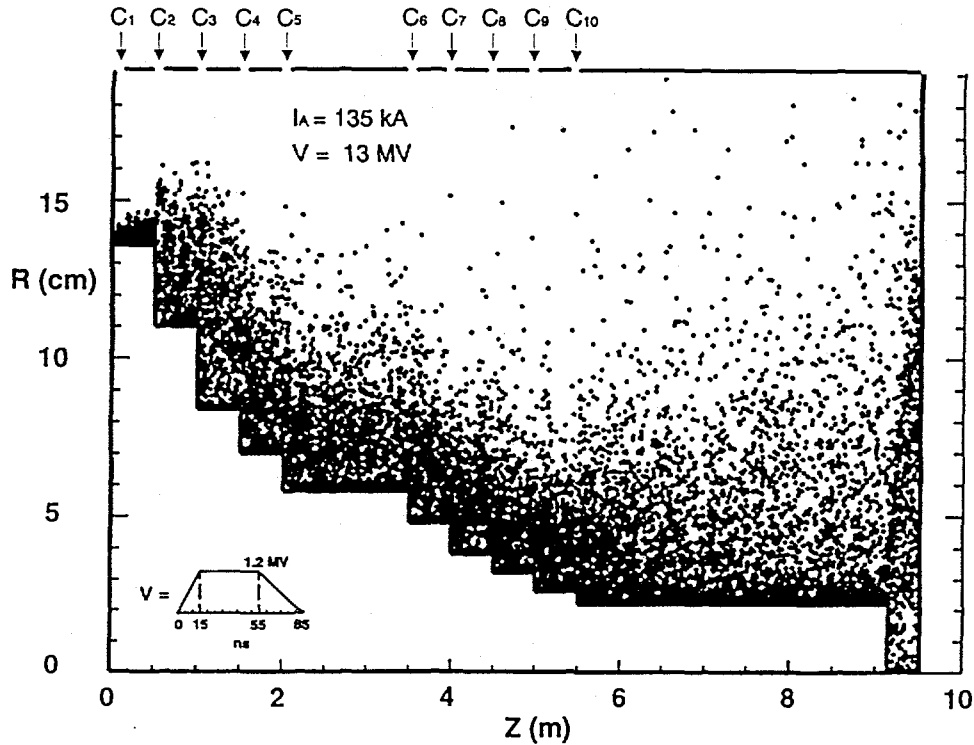

Figure 9. Electron map for the high impedance cathode electrode obtained with TWOQUICK PIC code at 60 ns following the arrival of the voltage pulse at the first cavity (t = 0).

Figure 10 is a simulation of the transition region. In this region all the sheath electrons are lost to the anode. The sum of the loss current and beam current is equal to the total current flowing along the voltage adder. Thus the transition region is the effective load for the SABRE MITL with an impedance equal to the MITL operating impedance (matched load). The location of the taper relative to the shape and strength of the solenoidal fringe field is very critical. Figure 10 shows the configuration that produces the highest brightness and lowest emittance beam. The magnetic field lines are also shown. The losses near the conically tapered section are due to the radial component B_r of the applied solenoidal magnetic field. They occur at the point where the self field B_θ becomes equal to the B_r component of the applied field. The applied B field was calculated for the actual coil configuration using the Atheta code which includes diffusion into the various materials based on their electrical conductivities. As seen in Fig. 10, the current splits, with about 70% striking the anode wall which is lined with a graphite insert to prevent activation of the stainless steel cylinder. The remaining 36 kA form a

pencil-like beam of about 0.6-mm radius. The resolution of the simulation is not fine enough to give the precise beam parameters.
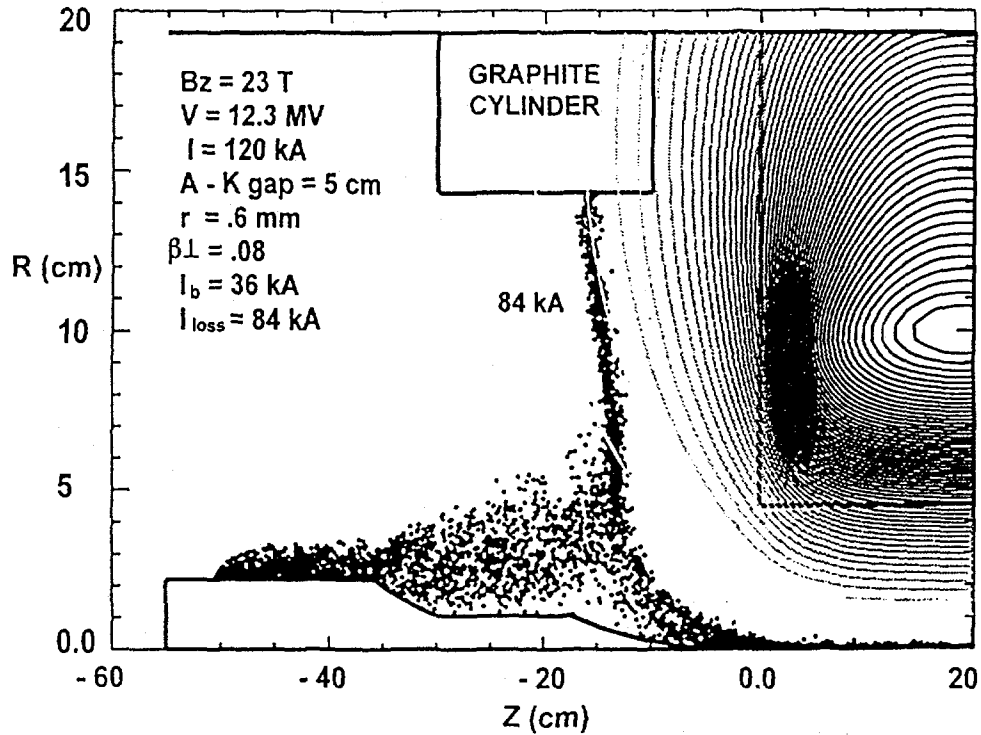

Figure 10. TWOQUICK simulation of the transition region. The losses near the conically tapered section are due to the radial component B_r of the applied solenoidal magnetic field.

The simulation of Fig. 11 was done with the above concern in mind, so only the immersed diode was included. The applied magnetic field B is the actual one, and the anode-cathode voltage is 12 MV. A beam of 36 kA with 0.44 mm rms radius is produced. This beam is the ultimate goal of the proposed experiments. This simulation represents an ideal situation assuming no cathode plasma radial expansion, perfect cylindrical symmetry without instabilities, and negligible beam perturbation due to possible beam-stop plasma blow offs. Some inconclusive scoping studies of those problems have been done up to now; however, only the experiments will tell how "ideal" is the simulated beam. According to the simulations, we should produce a beam with emittance $\varepsilon = \pi.r_b.\beta_\perp = 5 \ 10^{-5}$ m.rad. The brightness $B = 3.10^{13}$ A / (m.rad)^2 is calculated from the expression:

$$B = 2I / \varepsilon^2, \tag{4}$$

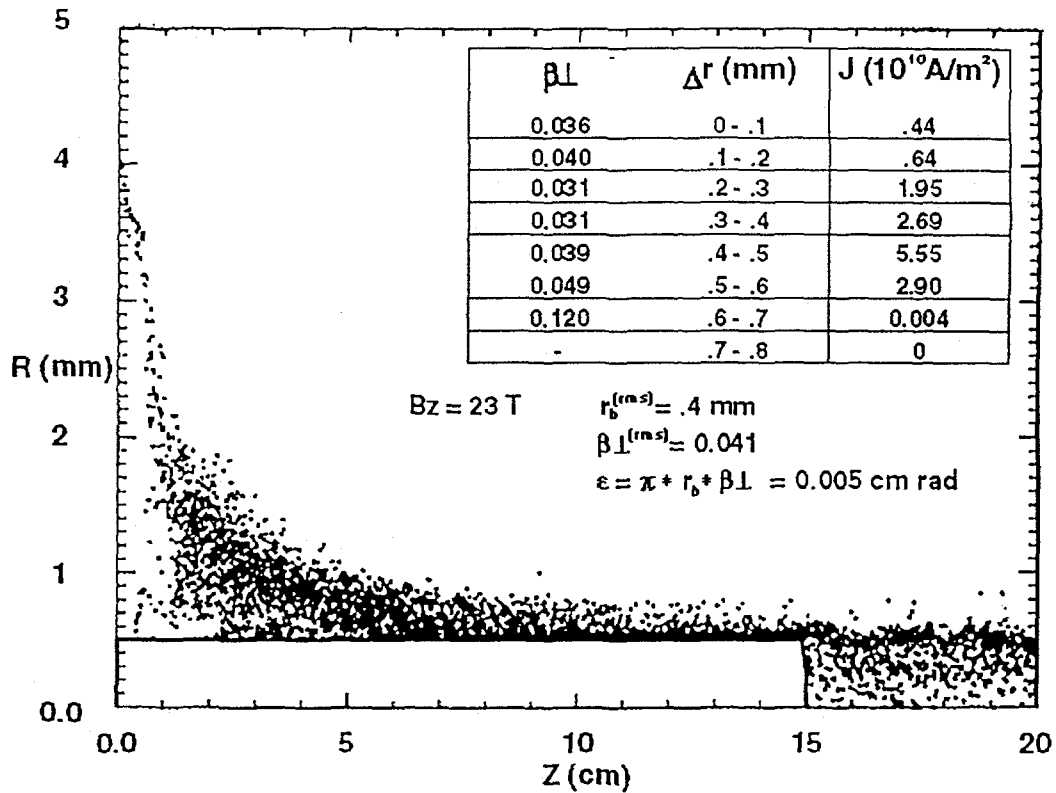where I is the beam current and ε the geometric emittance.

Figure 11.   High resolution diode simulation evaluating the beam parameters.

Figure 12 is the v_θ, Z phase space. The maximum rotation velocity is close to the speed of light. Figure 13 provides an interesting insight and comparison between the electrons self-field and the applied field. The electrons exhibit a strong rotation at the transition region and around the cathode electrode with a net diamagnetic component; however, the beam rotates much slower, and its diamagnetism is smaller and becomes zero at the beam stop. The phase space of Fig. 12 corresponds to the motion of the electrons of Fig. 10: the electrons escaping radially from the cathode electrode initially have a strong rotation because they cross the magnetic field lines while accelerated by the radial electric field. At Z = +20 cm (end of cathode tip), the electric field becomes axial, the electrons accelerate forward and their v_θ decreases.
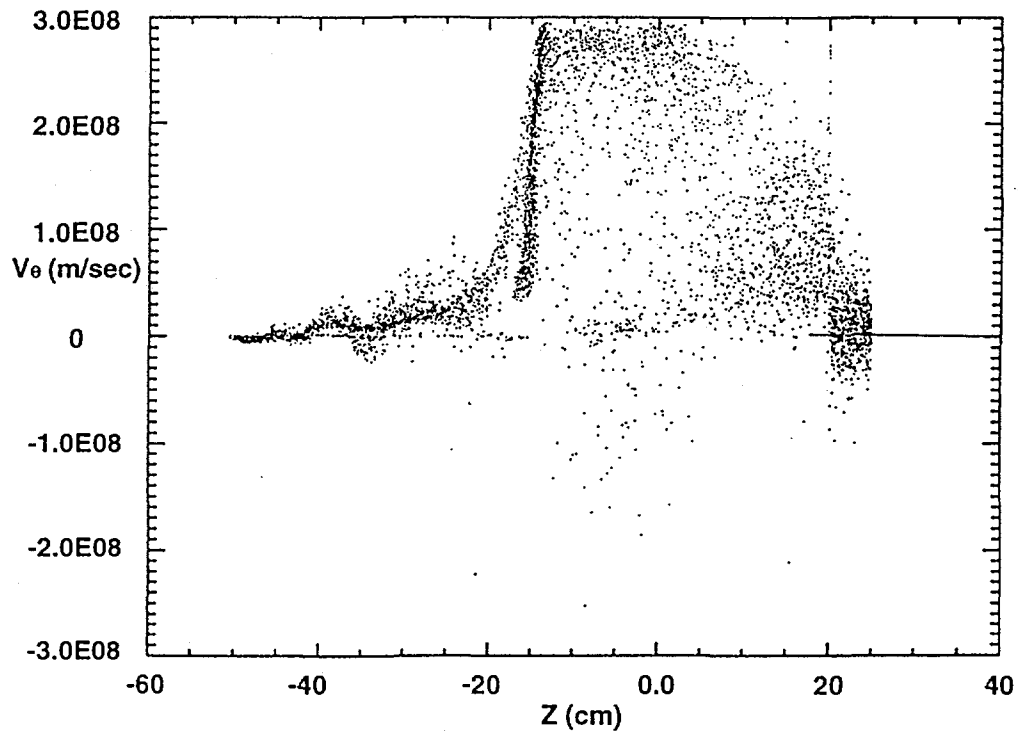
Figure 12. V_θ, z phase space of diode and transition region. It corresponds to the electron map of Figure 10.   In the transition region and around the cathode tip the V_θ can be as high as the speed of light. However, in the beam (z = 20-25 cm) the electrons rotate much slower ~ $V_\theta = 0.10$ V_c.
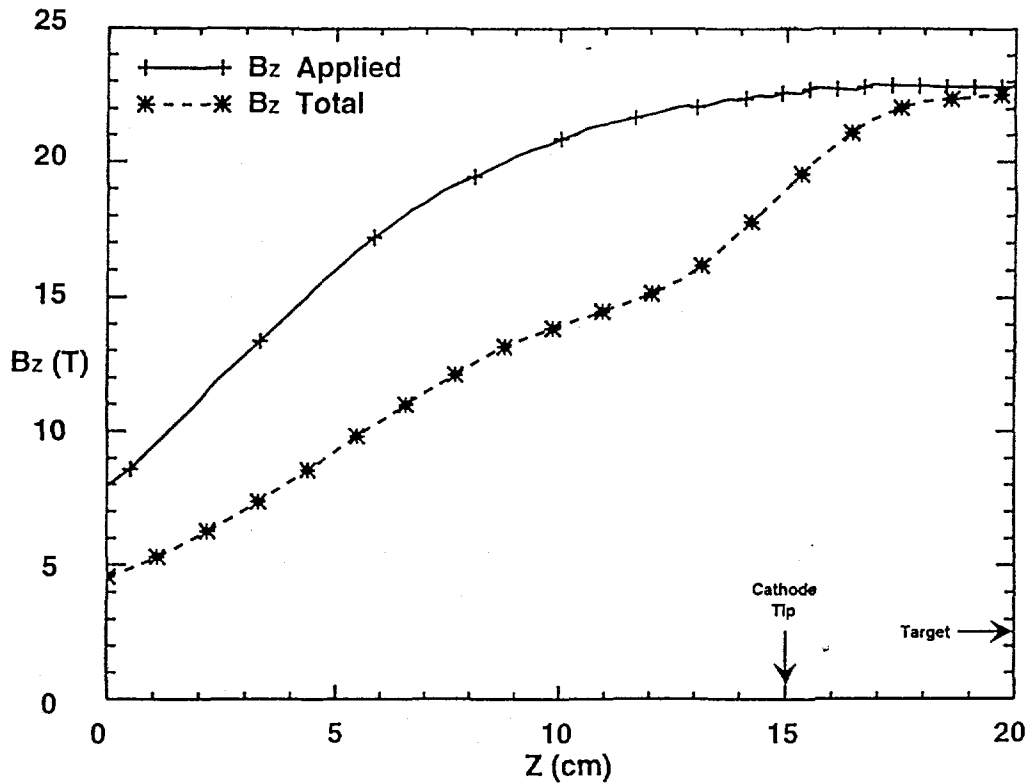
Figure 13. Applied and total B_z field at r = 0.5 mm (cathode tip radius).

The simulated beams are very tightly focused, depositing on the target very impressive amounts of energy per unit surface area. For instance, the current density, power density, and energy density are, respectively, $5.5 \ 10^6$ A/cm^2, $6.0 \ 10^{13}$ W/cm^2, $2.4 \ 10^6$ J/cm^2. Also the energy absorbed by the surface of a heavy metal target is of the order of 6×10^5 J/gr. This makes our beams ideal for beam-target-plasma interaction studies.

Summary

We have designed and constructed an immersed diode and a high impedance voltage adder for SABRE which, if they perform as expected, should produce a very intense high brightness electron beam of millimeter size. Extensive numerical simulations and previous experience with RADLAC II/SMILE suggests that these beams should be achievable. Halo, radial plasma expansion at the cathode and instabilities may limit the minimum possible beam radius. Experimental verification of the design and numerical simulation predictions is planned for the beginning of 1996. Experimental results will be reported in future publication.

References

1. T. M. Martin, *IEEE Trans. Nucl. Sci.* **NS-16**, 59 (1969).

2. J. J. Ramirez, J. P. Corley, and M. G. Mazarakis, *Proceedings of the 5th International Conference on High-Power Particle Beams*, San Francisco (Physics International, San Leandro, CA, 1983), p. 256.

3. R. B. Miller, K. R. Prestwich, J. W. Poukey, B. G. Epstein, J. R. Freeman, A. W. Sharpe, W. K. Tucker, and S. L. Shope, *J. Appl. Phys.* **52**, 1184 (1981).

4. M. G. Mazarakis, G. T. Leifeste, R. S. Clark, C. A. Ekdahl, C. A. Frost, D. E. Hasti, D. L. Johnson, R. B. Miller, J. W. Poukey, K. R. Prestwich, S. L. Shope, and D. L. Smith, *Proceedings of the 1987 IEEE Particle Accelerator Conference*, Washington, DC (IEEE, New York, 1987), p. 908.

5. M. G. Mazarakis, J. W. Poukey, S. L. Shope, C. A. Frost, B. N. Turman, J. J. Ramirez, and K. R. Prestwich, *Proceedings of the 8th International IEEE Pulsed Power Conference*, San Diego, CA, (IEEE, New York, 1991), p. 86.

6. D. E. Hasti, J. J. Ramirez, P. D. Coleman, C. W. Huddle, A. W. Sharpe, L. L. Torrison, *Proceedings of the 5th International IEEE Pulsed Power Conference*, Arlington, VA (IEEE, New York, 1985), p. 147.

7. L. M. Friedman and M. Ury, *Rev. Sci. Instrum.* **41**, 1334 (1970).

8. J. J. Ramirez, K. R. Prestwich, E. L. Burgess, J. P. Furaus, R. A. Hamil, D. L. Johnson, T. W. L. Sanford, L. E. Seamons, L. X. Schneider, and G. A. Zawadzkas, *Proceedings of the 6th International IEEE Pulsed Power Conference*, Arlington, VA (IEEE, New York, 1987), p. 294.

9. J. Corley, J. A. Alexander, P. J. Pankuch, C. E. Heath, D. L. Johnson, J. J. Ramirez, and G. J. Denison, *Proceedings of the 8th International IEEE Pulsed Power Conference*, San Diego, CA (IEEE, New York, 1991), p. 920.

10. J. H. Creedon, *J. Appl. Phys.* **48** (3), 1070 (1977).

11. N. Christophilos, R. E. Hester, W. A. S. Lamb, D. D. Reagan, W. A. Sherwood, and R. E. Wright, *Rev. Sci. Instrum.* **35** (7), 886 (1964).

12. T. W. L. Sanford, J. W. Poukey, T. P. Wright, J. Bailey, C. E. Heath, and R. Mock, *J. Appl. Phys.* **63** (3), 681 (1988).

13. M. G. Mazarakis, R. B. Miller, and J. W. Poukey, *J. Appl. Physics* **62** (10), 4024 (1987).

14. R. S. Coats, ATHETA/DATHETA User's Guide (Sandia National Laboratory document, Albuquerque, NM, 1995).

15. D. B. Seidel, M. L. Kiefer, R. S. Coats, T. D. Pointon, J. P. Quintenz, and W. A. Johnson, *Proceedings of the CP90 Europhysics Conference on Computational Physics*, Singapore (World Scientific, Singapore, 1991), p. 475.